Available online at www.sciencedirect.com
SCIENCE DIRECT
Polymer 46 (2005) 1661–1674
polymer
www.elsevier.com/locate/polymer

Reactively compatibilised polyamide6/ethylene-co-vinyl acetate blends: mechanical properties and morphology

Arup R. Bhattacharyya[a,1], Anup K. Ghosh[a], Ashok Misra[a,*], K.-J. Eichhorn[b]

[a]*Centre for Polymer Science and Engineering, Indian Institute of Technology Delhi, New Delhi 110016 India*
[b]*Department of Analysis, Leibniz Institute of Polymer Research Dresden, Hohe Strasse 6, D-01069 Dresden, Germany*

Received 27 May 2004; received in revised form 10 November 2004; accepted 9 December 2004

Abstract

Mechanical properties and morphological studies of compatibilised blends of PA6/EVA-*g*-MA and PA6/EVA/EVA-*g*-MA were studied as functions of maleic anhydride content (MA) and dispersed phase (EVA-*g*-MA) concentrations, respectively at blending composition of 20 wt% dispersed phase (EVA-*g*-MA or combination of EVA and EVA-*g*-MA). The maleic anhydride (MA) was varied from 1 to 6 wt% in the PA6/EVA-*g*-MA blend, whereas MA concentration was fixed at 2 wt% in the ternary compositions with varying level of EVA-*g*-MA. ATR-IR spectroscopy revealed the formation of in situ copolymer during reactive compatibilisation of PA6 and EVA-*g*-MA. It was found that notched Izod impact strength of PA6/EVA-*g*-MA blends increased significantly with MA content in EVA-*g*-MA. The brittle to tough transition temperature of reactively compatibilised blends was found to be at 23 °C. The impact fractured surface topology reveals extensive deformation in presence of EVA-*g*-MA whereas; uncompatibilised PA6/EVA blend shows dislodging of EVA domains from the matrix. Tensile strength of the PA6/EVA-*g*-MA blends increased significantly as compared to PA6/EVA blends. Analysis of the tensile data using predictive theories showed an enhanced interaction of the dispersed phase and the matrix. It is observed from the phase morphological analysis that the average domain size of the PA6/EVA-*g*-MA blends is found to decrease gradually with increase in MA content of EVA-*g*-MA. A similar decrease is also found to observe in PA6/EVA/EVA-*g*-MA blends with increase in EVA-*g*-MA content, which suggest the coalescence process is slower in presence of EVA-*g*-MA. An attempt has been made to correlate between impact strength and morphological parameters with regard to the compatibilised system over the uncompatibilised system.

Keywords: Reactive compatibilisation; Mechanical properties; Morphology

1. Introduction

A majority of polymer blends are thermodynamically immiscible in nature due to the low entropy of mixing [1]. In binary blends, the unfavourable entropy of mixing, leads to coarse and unstable phase morphology with high interfacial tension and low interfacial adhesion [2]. As a result, the mechanical properties of immiscible polymer blends are inherently inferior in nature. The introduction of block or graft copolymers suitably modifies the interface, which in turn stabilise the phase morphology [3–5]. However, this strategy cannot be applied to all kinds of blends, and moreover, the synthesis of block or graft co-polymer is often very expensive. In recent times, considerable attention has been focused on reactive compatibilisation [4,6–17], which is based on the in situ formation of a block or graft copolymer at the interface during melt blending. This technique is very often used to stabilise the morphology of the immiscible polymer blends to obtain appropriate mechanical properties.

In this context, a large number of literatures are available on the reactive compatibilisation of rubber modified polyamide6 (PA6) blends [18–22]. These studies have focused on the correlation between impact toughening and the nature of rubbery phase along with various factors,

* Corresponding author. Present address: Director, Indian Institute of Technology Bombay, Powai, Mumbai 400076, India. Tel.: +91 22 576 7001; fax: +91 22 572 3546.
E-mail address: amisra@iitb.ac.in (A. Misra).
[1] Present address: Department of Metallurgical Engineering and Materials Science, Indian Institute of Technology Bombay, Powai, Mumbai 400076, India.

0032-3861/$ - see front matter © 2004 Elsevier Ltd. All rights reserved.
doi:10.1016/j.polymer.2004.12.012

which affect the development of morphology (e.g. degree of maleation, processing parameters, viscosity ratio). The nature of matrix molecular weight on the impact toughening has been investigated in detail by Paul and co-workers [23–25]. Enhanced interfacial adhesion with improved fracture toughness has been achieved in PP/PA6 blends utilising PP-*g*-MA as a reactive compatibiliser [26]. Morphology, mechanical properties and rheology have been studied in the blends of PPO/PA6 with functionalised elastomers [27]. Effect of styrene maleic anhydride copolymer driven reactive compatibilisation on phase morphology and the stability of the co-continuous blends of (PPE/PS)/PA6 and PS/PA6 have been reported in the literature [28]. The effect of the concentration of reactive functional group during reactive compatibilisation of PBT and epoxide containing rubber has been reported [29]. The effect of reactive compatibilisation in PA6/LDPE blends in presence of ethylene acrylic acid and a low molar mass bis-oxazoline has been reported [30]. Effect of reactive compatibilisation by imidized acrylic polymer on the tensile stress–strain behaviour and morphology has been reported for PA6/SAN blends [31]. Cooperative toughening and cooperative compatibilisation has been reported in case of ethylene acrylic acid compatibilised PA6/EVA blends [32]. Effect of reactive compatibilisation on the interfacial slip in PA6/EPR blends has been studied by Groeninckx and co-workers [33]. Morphology and mechanical properties of PBT/PA6/EVA-*g*-MA ternary blends have been reported by Kim et al. [34]. The in situ compatibilisation of PET copolymer (PETG) with EVA via dibutyltin oxide catalysed transesterification reactions was studied through rheological, morphological and mechanical studies [35]. In another important study morphological modification of PBT/PE/EVA ternary blends by transesterification precursor induced interfacial chemical reaction has been demonstrated [36].

Ethylene vinyl acetate grafted with maleic anhydride (EVA-*g*-MA) has been found effective as a reactive compatibiliser in PA6/EVA and PBT/EVA blends [37–39]. It is also to be pointed out that there are very few literatures available on PA6/EVA blends where EVA-*g*-MA has been utilised as a reactive compatibiliser. In one of our earlier publications, the effect of EVA-*g*-MA on phase morphology and crystallisation behaviour was demonstrated successfully in PA6/EVA blends system [37].

The aim of the paper is to address the effects of reactive compatibilisation using EVA-*g*-MA on the mechanical properties and morphology of the binary and ternary blends of PA6, EVA and EVA-*g*-MA. ATR-IR spectroscopy was carried out to investigate the formation of in situ copolymer during reactive compatibilisation of PA6 and EVA-*g*-MA. Mechanical properties such as temperature dependent impact strength were studied as functions of MA concentration and EVA-*g*-MA level in the binary and ternary blends. Tensile behaviour was analysed using predictive models in order to assess the interfacial interaction in the presence of EVA-*g*-MA. An attempt has also been made to correlate the impact properties and the morphological parameters.

2. Experimental

2.1. Materials

Polyamide6 (PA6) with a zero shear viscosity of 1211 Pa s was obtained from Gujarat State Fertilizer Corporation, Baroda, India (GUJLON M28RC, relative viscosity 2.8, M_v is 38,642 in 85% formic acid). Ethylene vinyl acetate (EVA) with vinyl acetate content of 18% and melt flow index of 2 gm/10 min having a zero shear viscosity of 5999.7 Pa s (EVA 1802, supplied by National Organic Chemical Industries Limited, Mumbai, India) was used as blending polymer. The EVA grafted with maleic anhydride (EVA-*g*-MA) was prepared in a corotating, intermeshing twin screw extruder (ZSK25) in the temperature range of 150–160 °C at 150 rpm by varying the level of MA (1–6 wt%) using styrene and benzoyl peroxide (BPO). EVA-*g*-MA was purified to remove unreacted MA and the procedure has been described in the subsequent section of IR spectroscopic analysis. The percentage grafting of MA on EVA (EVAG1 and EVAG2 where initial MA content was 1 and 2 wt%, respectively) was determined by an elemental analyser (C.E. Instruments, Eager 300 EA1112) from measuring the oxygen content of MA grafted onto EVA as reported in reference [38]. It was found that in case of EVAG1 and EVAG2 the % MA grafted on EVA is 0.45 and 1.12, respectively. In order to minimize side reactions (crosslinking between EVA chains) and improving grafting efficiency, styrene as a co-monomer was employed. The competition between crosslinking reactions between EVA chains and the grafting of MA on EVA in the presence of a peroxide initiator during melt free radical grafting of MA on EVA has been reported in detail [38–39]. In this context, the use of a comonomer during melt free radical grafting has been found effective to improve the grafting efficiency in several polymer systems (PE, PP, EPR) [40–41]. In this context it is to be mentioned that gel content was not determined in case of EVA-*g*-MA. The polymers were dried in a vacuum oven at 80 °C for over 24 h to ensure removal of moisture.

2.2. Blending and preparation of test specimen

The granules were dry-mixed in appropriate ratios and the binary as well as ternary blends of PA6, EVA and EVA-*g*-MA were prepared in a corotating, intermeshing twin screw extruder (ZSK25, $L/D=46$) with a screw speed of 150 rpm at 230 °C. In this context it is to be pointed out that the residence time was approximately 2–3 min for preparing the blends of PA6 and EVA-*g*-MA. It is found from the literature that 2–3 min of residence time in a twin screw extruder is sufficient for reactive coupling to take place

between the amine end group of PA6 and the anhydride functionality of MA which gives rise to stable morphology [42]. The level of EVA, or EVA-*g*-MA was fixed at 20 wt% in the binary blends of PA6/EVA and PA6/EVA-*g*-MA, respectively. In the ternary blends of PA6/EVA/EVA-*g*-MA, the level of EVA-*g*-MA (2 wt% MA) was varied from 10 to 15 wt% keeping the overall ratio of PA6 and EVA plus EVA-*g*-MA at 80/20. The detailed blend compositions are given in Table 3. The extruded strands were quenched immediately after extrusion in a water bath kept at room temperature. The extruded strands were then chopped into granules and finally dried at 80 °C for over 24 h before moulding. The component polymers were also extruded in the same way so that they would have the same history as the blend compositions. Test specimens for determining the mechanical properties were prepared by injection moulding at 230 °C and at a screw speed of 80 rpm (Windsor SP-1).

2.3. Characterisation

2.3.1. IR spectroscopic analysis

2.3.1.1. Grafting of MA on EVA. FTIR spectroscopy was carried out for purified EVA-*g*-MA samples where MA concentration was varied from 1 to 2 wt%. EVA-*g*-MA was purified to remove unreacted MA from the system by the following way. Unpurified EVA-*g*-MA was initially dissolved in boiling xylene and subsequently precipitated in acetone, where unreacted MA would dissolve. The precipitate was washed with acetone several times and dried. The same process has been adopted for pure EVA as well. Samples prepared as thick melt films, pressed at 145 °C, thickness about 250 μm, measured in transmission on a Bruker IFS 66v/S spectrometer with DTGS detector, resolution 2 cm^{-1}, 32 scans /spectrum, all absorbance spectra are baseline corrected.

2.3.1.2. Determination of copolymer formation. To determine the copolymer formation during reactive blending of PA6 and EVA-*g*-MA, the following procedures were adopted to prepare the samples for ATR-IR analysis. PA6/EVA-*g*-MA blends (NG1 and NG4) were dissolved in boiling xylene and the soluble part (EVA-*g*-MA) was subsequently precipitated in acetone and the precipitate (EVA-*g*-MA) washed with acetone and dried. One composition of PA6/EVA-*g*-MA blends (NG2) was dissolved in formic acid and the soluble part subsequently precipitated in acetone and the precipitate (PA6) washed with acetone and dried. In case of unreactive blends of PA6 and EVA (N20), the EVA part was extracted by dissolving the blends sample in boiling xylene and the soluble part subsequently precipitated in acetone and the precipitate (EVA) washed in acetone and dried. All the samples were measured with ATR technique, Golden Gate Diamant ATR, on a Bruker IFS 66v/S spectrometer with MCT detector, resolution 4 cm^{-1}, 100 scans/spectrum. All the spectra are baseline corrected and shown as absorbance like ATR units.

2.3.2. Wide angle X-ray diffraction (WAXD)

WAXD studies were carried out on a Rigaku Rotaflex Ru-200B, rotating anode operated at 40 kV and 100 mA, and equipped with a Kratky camera. The incident X-rays ($\lambda = 1.54$ Å) from the Cu-target were monochromatized using a Ni filter. Compression moulded samples of 1 mm thickness were used as test specimens. WAXD patterns were recorded in transmission mode with a step scan with step size of 0.050 between 10 and 30° 2θ. Degree of crystallinity (X_c) was calculated from the diffractograms obtained using the following relation:

$$X_c = \{S^2 I_{cr}(S)\}dS/\{S^2 I(S)\}dS$$

where $I_{cr}(S)$, the coherent intensity concentrated in the crystallization peak; $I(S)$, the total coherent intensity scattered; S, scattering vector, expressed as $S = (2/\lambda)\sin\theta$.

The crystallite size in the direction perpendicular to (002) and (202) planes was determined by using Scherrer's equation:

$$L_{hkl} = K'/\beta\cos\theta$$

where L_{hkl}, mean dimension of the crystallite along the direction perpendicular to *hkl* lattice plane; β, breadth at half height of the diffraction maxima corresponding to *hkl* planes (on 2θ scale) in radians; K', constant whose value is generally taken as unity or more precisely as 0.89, and is related to crystallite shape.

2.3.3. Differential scanning calorimetry (DSC)

DSC measurements were carried out for all the blends and the pure polymers using Perkin Elmer DSC 7. The extruded samples of about 5 mg were dried in a vacuum oven prior to experiment. Thermograms were recorded during both heating and cooling cycle at 10 °C/min using identical setting of instrument for all the samples. All the samples were first run through a heating cycle from 50 to 250 °C and then through a cooling cycle after holding for 2 min at 250 °C, to destroy any previous thermal history and crystallization. The cooling scans were used to determine the crystallization behaviour of the components of the blends, such as onset of crystallization (T_5), peak temperature of crystallization (T_6), completion of crystallization (T_7), width of crystallization exotherm (T_5–T_7) and heat of crystallization (ΔH_c).

2.4. Mechanical properties

Notched Izod impact strength was measured on CEAST impact tester (Model Resil 25) following ASTM D-256. All impact strength measurements were made at five different temperatures (−25, 0, 23, 40 and 80 °C). Tensile properties were measured on an Instron Universal Tester (Model 4301)

according to ASTM D-638, type 1 procedure at an extension rate of 50 mm/min. The test results reported are the average values of at least ten specimens tested in each case to get a reliable value and the deviation of the data around the mean value was less than 5%.

2.5. Morphology

Morphological studies were conducted by scanning electron microscopic (SEM) analysis using a Cambridge Stereoscan Microscope (Model S4-10). Impact fractured (at 23 °C) specimens were used in order to investigate the fracture surface of the blends. Cryogenically fractured etched tensile specimens were used for phase morphological analysis. The etching was carried out by *o*-xylene to remove EVA (or EVA-*g*-MA) selectively from the respective blends samples. For each blends, different micrographs were made and were analysed by image analyser to determine the average domain size. Number average diameter (D_n) and weight average diameter (D_w) of the domain were determined according to the following relationships:

$$D_n = \sum N_i D_i / \sum N_i \quad (1)$$

$$D_w = \sum N_i D_i^2 / \sum N_i D_i \quad (2)$$

The critical inter-particle distance was calculated form Wu's equation:

$$\text{IPDC} = d[(3.14/6\varphi_r)^{1/3} - 1] \quad (3)$$

where d is the average diameter of the domain and ϕ_r is the volume fraction of the dispersed phase.

3. Results and discussion

3.1. IR spectroscopic analysis

FTIR spectroscopy was carried out to identify the characteristics peaks of MA, which is grafted onto EVA. Fig. 1 shows the extended spectral region (1600–1900 cm^{-1}) of EVA and EVA-*g*-MA. It shows that the characteristics peaks of MA appeared at 1780 and 1857 cm^{-1} in EVA-*g*-MA whereas; these two peaks are absent in EVA. In addition, it is also to be pointed out that the intensity of the two peaks are found to be stronger in case of EVA-*g*-MA where MA concentration was 2 wt%. This suggests that the amount of MA grafted on EVA is more with increase in MA concentration. In this context, it is also to be pointed out that quantitative measurements were also carried out to determine the % grafting of MA on EVA in EVAG1 and EVAG2. It was found that in case of EVAG1 and EVAG2 the % MA grafted on EVA is 0.45 and 1.12, respectively which is again in favour of IR spectroscopic analysis.

In addition, extraction experiments were performed to verify the formation of PA6-*g*-EVA copolymer, which would be expected during the reactive compatibilisation of the blends of PA6 and EVA-*g*-MA. Fig. 2 shows the extended spectral region (1400–2000 cm^{-1}) of ATR-IR spectra of pure PA6, EVA soluble part of NG1 and NG4 together with PA6 soluble part of NG2. In case of pure PA6, the amide peaks are found to appear at 1635 and 1537 cm^{-1} corresponding to amide-I and amide-II. It also indicates that the characteristics peaks of amide-I and amide-II appear at 1635 and 1537 cm^{-1}, respectively, whereas ester C=O stretch is found to appear at 1735 cm^{-1} for all the extracted samples of PA6/EVA-*g*-MA blends. This suggests that even after extraction bands corresponding to PA6 and EVA are found to appear in all the extracted samples of reactive blends, which is an indication of copolymer formation in the presence of EVA-*g*-MA. In addition, Fig. 3 shows the characteristics peak of N–H stretching at 3287 cm^{-1} of pure PA6 together with all the extracted samples of PA6/EVA-*g*-MA blends, which again indicates the formation of PA6-*g*-EVA copolymer during reactive blending between PA6 and EVA-*g*-MA. In contrast, the EVA soluble part of the unreactive blends of PA6/EVA (N20) shows characteristics peaks corresponding to pure EVA in the ATR-IR spectra (not shown here). Based on the above experimental

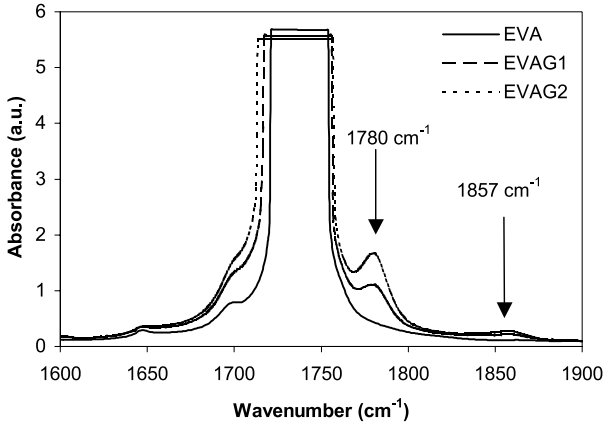

Fig. 1. FTIR spectra of EVA and EVA-*g*-MA.

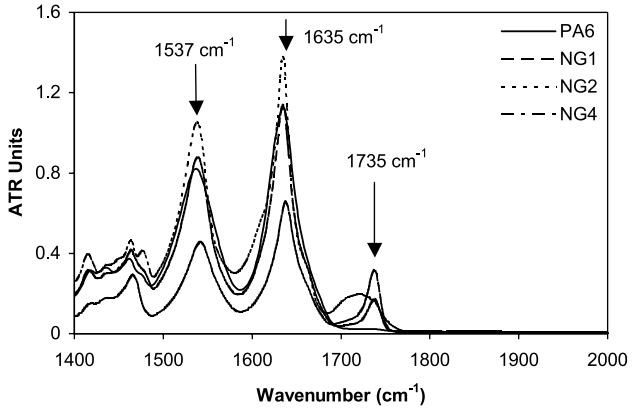

Fig. 2. ATR-IR spectra of pure PA6 and the extracted samples of PA6/EVA-*g*-MA blends, spectral range 1400–2000 cm^{-1}.

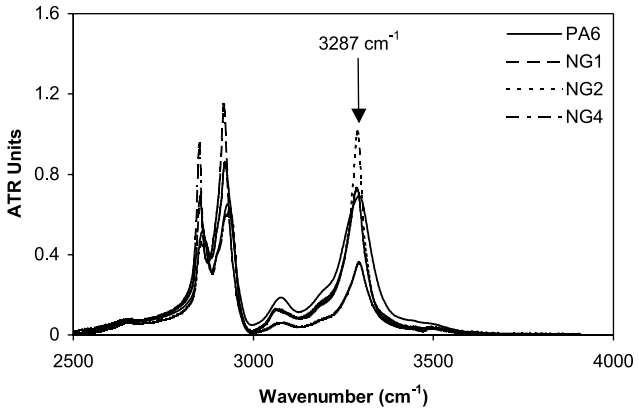

Fig. 3. ATR-IR spectra of pure PA6 and the extracted samples of PA6/EVA-*g*-MA blends, spectral range 2500–4000 cm^{-1}.

observation and the available literature [31] the following compatibilisation mechanism can be proposed and can be illustrated schematically as:

(a) grafting of MA onto EVA in presence of styrene:

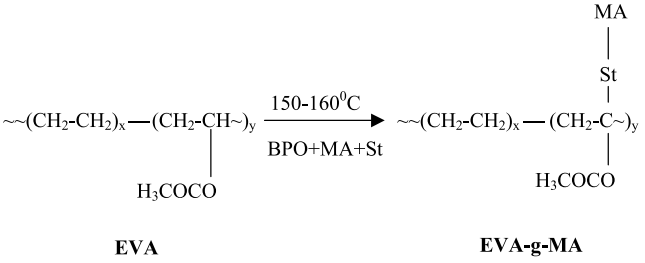

(b) interfacial reaction between EVA-*g*-MA and the PA6:

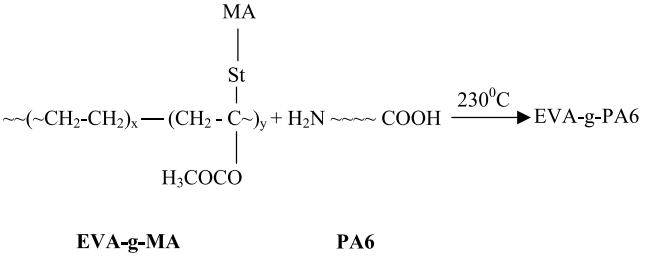

3.2. Crystallisation behaviour: WAXD and DSC analysis

The diffraction parameters (intensity maxima *I*, crystallite size *L*, overall crystallinity Xc) obtained from wide angle X-ray diffraction patterns (Fig. 4) of PA6 and the blends of PA6/EVA and PA6/EVA-*g*-MA are given in Table 1.

Pure PA6 usually crystallises into the α-crystalline form corresponding to 200, 002 and 202 reflections. Two sharp diffraction maxima at 2θ values of 21.2° (200 reflection) and 23.7° (002 and 202 doublet) are present in the diffraction pattern of PA6 characteristics of α-crystalline form of PA6.

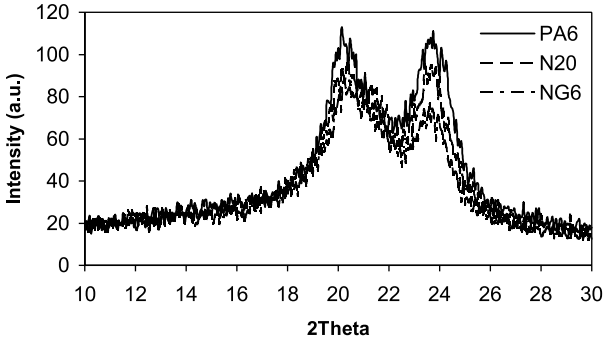

Fig. 4. Wide angle X-ray diffractograms of PA6 and its blends.

Similarly, EVA shows two peaks at 21.2 and 22.8°. The blends of PA6/EVA show again the presence of two peaks. It is believed that the diffraction pattern of the blends is a superposition of PA6 and EVA diffraction pattern. It is observed that the peak positions (2θ) of the blends are relatively unaffected at 20 wt% EVA level. This observation has also been noticed in case of reactively compatibilised PA6/EVA blends. This suggests that the *d*-spacing corresponding to the specific plane remain unaltered, i.e. the dispersed phase is not been accommodated in the intraspherulitic region. The crystallite size in the direction perpendicular to 200 reflection is found to decrease considerably on incorporation of 20 wt% EVA (or EVA-*g*-MA). The overall crystallinity of the reactively compatibilised blends decreased as compared to both uncompatibilised blends and that of pure PA6. This suggests the mobility of the crystallising chains is substantially reduced due to the graft copolymer formation at the interface, which indicates the hindrance of crystallisation of both the phases. This observation is again in favour of evidence found from differential scanning calorimetric analysis for PA6/EVA-*g*-MA blends [37].

Fig. 5 shows the crystallisation exotherms of EVA-*g*-MA and the blends of PA6/EVA-*g*-MA. It is evident from Table 2 that the crystallisation peak temperature of EVA-*g*-MA decreased significantly on increasing the MA content in EVA-*g*-MA with lower heat of crystallisation. This suggests the hindrance of EVA chains in presence of MA moiety. The lowering of heat of crystallisation of EVA-*g*-MA in the blends of PA6/EVA-*g*-MA with higher MA content suggests the formation of graft copolymer between the amine end group of PA6 and anhydride functionality in the interface. This graft copolymer, in turn, affects the mobility of EVA chain thus lowering the crystallisation. In brief, the reactively compatibilised PA6/EVA-*g*-MA blends are separately crystallising at the bulk temperature of crystallisation of their individual components accompanied by lower heat of crystallisation.

3.3. Impact properties

The notched impact strength values for the blends

Table 1
Wide angle X-ray diffraction parameters

Sample Code	I_1 (Arb. unit)	I_2 (Arb. unit)	I_1/I_2	$2\theta_1$	$2\theta_2$	L_1 (Å)	L_2 (Å)	$\%X_c$
PA6	113	111	1.01	21.2	23.7	26.0	26.2	52.8
N20	100	94	1.06	20.4	23.8	18.5	28.9	45.6
NG1	100	97	1.03	20.7	23.7	15.7	32.6	44.0
NG2	100	84	1.20	20.4	23.8	17.9	24.8	42.5
NG4	90	86	1.04	20.4	23.5	20.0	28.9	39.0
NG6	87	77	1.12	20.2	23.6	17.9	26.0	35.8

studied at 23 °C are given in Table 3. It has been shown earlier that the addition of EVA copolymer to PA6 increases the notched impact strength of PA6 to a limited extent due to immiscibility/incompatibility with the two polymers [43]. On addition of 20 wt% EVA, the notched impact strength of the PA6/EVA blends increased by a factor of about two as compared to pure PA6 at 23 °C, however, the impact strength of the blends still remains in the brittle regime. The blends, which exhibit notched Izod impact strength below 200 J/m, are regarded as brittle blends whereas, those exhibit higher than 500 J/m are regarded as tough blends [18]. In this context, the use of EVA-*g*-MA has been found effective in PA6/EVA blends [37]. It is reported that at 23 °C, the notched impact strength of the PA6/EVA-*g*-MA blends increased at all levels of EVA-*g*-MA, the increase being 3.5–6.2 times that of 80/20 PA6/EVA depending on the MA level [37]. In this study the variation of notched impact strength of PA6/EVA-*g*-MA with MA content and the temperature dependent impact strength of PA6/EVA-*g*-MA and PA6/EVA/EVA-*g*-MA blends has been determined and presented in Figs. 6 and 7, respectively. It is found from Fig. 6 that the increase in impact strength is found maximum at 6 wt% MA level in PA6/EVA-*g*-MA blends. It is also observed that the impact strength increased significantly in PA6/EVA-*g*-MA blends at all temperatures as compared to uncompatibilised PA6/EVA blends. The variation in the notched impact strength of the blends with the MA level (or with the EVA-*g*-MA level in ternary compositions) was

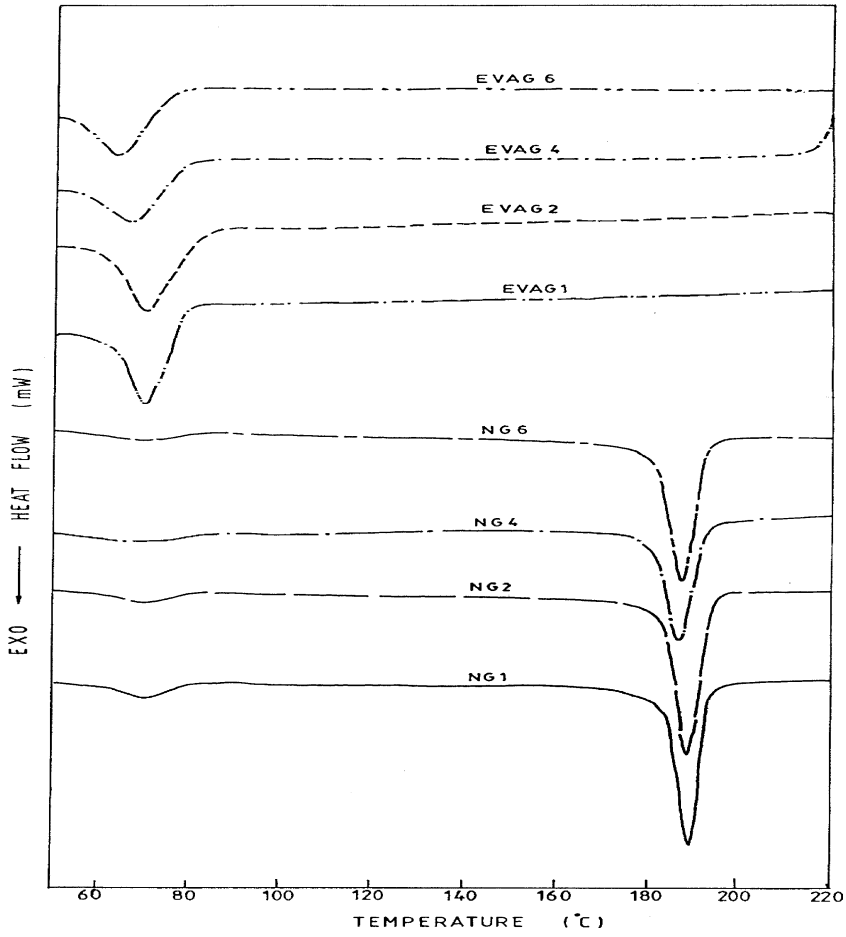

Fig. 5. DSC cooling scans of PA6/EVA and PA6/EVA-*g*-MA blends.

Table 2
DSC crystallisation parameters of EVA (EVA-*g*-MA) phase of PA6/EVA and PA6/EVA-*g*-MA blends

Sample code	Composition PA6/EVA/EVA-*g*-MA	Onset (T_5, °C)	Peak (T_6, °C)	Completion (T_7, °C)	Peak width (T_5–T_7)	ΔH_c (J/g)
EVA100	0/100/0	75.5	70.0	51.6	23.9	37.8
EVAG1	0/0/100	78.2	70.4	52.2	26.0	34.7
EVAG2	0/0/100	78.3	69.5	52.3	26.0	30.4
EVAG4	0/0/100	77.3	67.0	51.8	25.5	26.2
EVAG6	0/0/100	74.9	64.8	51.6	23.3	24.0
N20	80/20/0	78.5	71.3	60.2	18.3	24.8
NG1	80/0/20	78.6	70.2	53.2	25.4	35.8
NG2	80/0/20	79.7	70.3	54.7	25.0	27.9
NG4	80/0/20	81.4	71.3	53.4	28.0	27.2
NG6	80/0/20	80.5	70.0	54.7	25.8	21.1

generally similar at all test temperatures (Fig. 7). On increasing the test temperature, all the compositions showed higher values as compared to the values obtained at lower temperatures. Of special significance is the increase in impact strength at low temperatures. At −25 °C the increase is 3.9 to 6.3 times as compared to uncompatibilised PA6/EVA blends. However, all the values are still in the brittle regime. The brittle-to-tough transition temperature (T_{bt}) of these blend compositions shifted to 23 °C whereas, 80/20 combination of PA6/EVA blends showed the T_{bt} at 40 °C. In case of PA6/EVA/EVA-*g*-MA blends, the T_{bt} has also been found at 23 °C. The shift of T_{bt} may be explained on the basis of interparticle distance of the dispersed phase [18]. It is also reported in a number of systems based on PA66/rubber blends that critical interparticle distance is the important parameter that dictates T_{bt}. The values of critical interparticle distance are determined and are presented in the subsequent morphology section.

3.4. Impact fractured surface morphology

The SEM micrographs of the notched impact fractured surfaces of PA6/EVA-*g*-MA and PA6/EVA/EVA-*g*-MA blends together with PA6/EVA blends are presented in Fig. 8. As reported earlier PA6/EVA blends show debonding of EVA particles with hemispherical bumps indicating little adhesion between PA6 and EVA [43]. The 80/20 PA6/EVA blend is characterised by brittle fracture and there is no sign of plastic deformation or cavitation of EVA particles. On impact, only notch tip undergoes stress whitening. On the contrary, the entire fracture surface undergoes stress whitening in the reactively compatibilised blends. It is observed from Fig. 8 that reactively compatibilised blends exhibit rumples with shear bands formation in some compositions. This suggests that high rate of plastic deformation is associated with the fracture. In case of PA6/EVA-*g*-MA and PA6/EVA/EVA-*g*-MA blends, during impact the deformation is triggered by matrix (PA6) yielding where EVA-*g*-MA phase participated in the deformation process leading to the formation of extensive rumples and shear bands in some compositions. This is believed to be due to better interfacial adhesion between PA6 and EVA in the presence of maleic anhydride. Similar kind of observations has also been reported in other blends system by Speroni and co-workers [44]. This strongly suggests that on addition of EVA-*g*-MA, the interfacial adhesion between PA6 and EVA-*g*-MA improved significantly.

3.5. Phase morphology

The representative SEM micrographs of cryogenically fractured etched surfaces of PA6/EVA and PA6/EVA-*g*-MA blends are presented in Fig. 9. It has been reported earlier that the reactively compatibilised PA6/EVA blends are characterised by small domain size with narrow domain

Table 3
Mechanical properties of PA6/EVA-*g*-MA and PA6/EVA/EVA-*g*-MA blends

Sample code	Composition PA6/EVA/EVA-*g*-MA (wt%)	Impact strength (23 °C) (J/m)	Stress at peak (MPa)	Stress at break (MPa)	Strain at break (%)
PA6	100/0/0	72	50	43	273
N20	80/20/0	140	39	38	290
NG1	80/0/20 (MA = 1 wt%)	545	40	39	244
NG2	80/0/20 (MA = 2 wt%)	675	43	41	263
NG4	80/0/20 (MA = 4 wt%)	805	45	44	248
NG6	80/0/20 (MA = 6 wt%)	847	45	44	260
N80E10G10	80/10/10 (MA = 2 wt%)	588	43	42	277
N80E5G15	80/5/15 (MA = 2 wt%)	657	38	37	245

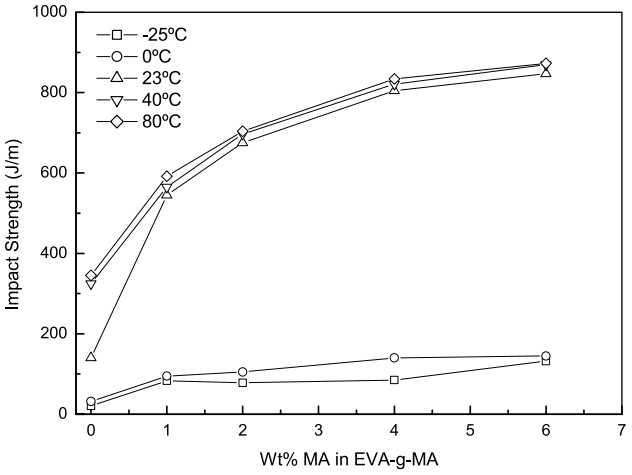

Fig. 6. Plot of impact strength versus MA content in EVA-*g*-MA for PA6/EVA-*g*-MA blends.

size distribution, higher interfacial thickness and immobile interface in contrast to large domain size and distribution, sharp and mobile interface in uncompatibilised blends [37].

From the micrographs it is seen that both the blends are characterised by dispersed particle type of morphology in which the minor component is dispersed in the form of spherical domains. It is observed from Fig. 10 that the average domain size (D_n and D_w) of the PA6/EVA-*g*-MA blends gradually decreases with increase in MA content in EVA-*g*-MA. Similar decrease was also found with an increase in the EVA-*g*-MA level in PA6/EVA/EVA-*g*-MA blends (Fig. 11). These observations suggest the coalescence process is slower in the presence of EVA-*g*-MA thus giving rise to fine dispersions of the minor phase. The formation of graft copolymer between amine end group of PA6 and anhydride functionality of MA is believe to reduce interfacial tension thus reducing the rate of coalescence.

According to Wu's theory [18], the brittle-to-tough transition temperature of the blends depends on the critical

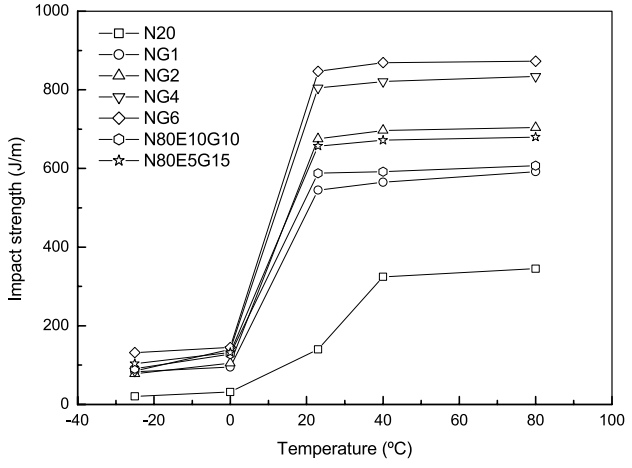

Fig. 7. Plot of impact strength versus temperature in PA6/EVA-*g*-MA and PA6/EVA/EVA-*g*-MA blends.

matrix ligament thickness (IPDC). If the matrix ligament thickness is lower than the critical value, the blends will be tough, while, if it is above the critical value, the blends will be brittle. It has also been reported that the critical value of the ligament thickness of PA6/rubber blends is about 0.3 μm. It is observed from Fig. 12 that the IPDC for the 80/20 PA6/EVA blends is higher (0.85 μm) than the critical value. Thus, the blends of PA6/EVA show brittle behaviour. In contrast, the IPDC for the PA6/EVA-*g*-MA blends is lower than 0.3 μm, which is giving rise to tough behaviour. This may explain the increase in impact strength and the change in brittle to tough transition temperature in PA6/EVA-*g*-MA blends as compared to PA6/EVA blends.

3.6. Correlation between impact strength and morphology

This section deals with the correlation between the impact strength and average domain size obtained from the phase morphological analysis of PA6/EVA and PA6/EVA-*g*-MA blends. Morphological studies of all PA6/EVA-*g*-MA based blends showed a two-phase morphology. It was found that on addition of EVA-*g*-MA of different levels of MA content the morphology of the binary and the ternary blends changed significantly. Comparing the two systems studied it can be clearly seen that compatibilisation has been very effective in modifying the phase morphology which leads to superior property profile. An attempt has been made to correlate the impact strength and the morphological parameters in the compatibilised system. The plot of the reduced domain size with the level of the compatibiliser (wt% MA) is presented in Fig. 13. The reduced domain size is defined as the ratio of domain size of EVA in compatibilised system to the domain size of EVA in uncompatibilised 80/20 PA6/EVA blends. Fig. 14 shows the dependence of impact strength in compatibilised system with reduced domain size. It is observed from this figure that a linear relationship of impact strength and domain size is observed in PA6/EVA-*g*-MA blends. Finally, an attempt has been made to correlate between the relative impact strength and the reduced domain size as presented in Fig. 15. It is clearly observed that a linear correlation exists between relative impact strength and the reduced domain size, which clearly demonstrate the effect of compatibilisation, which in turn enhances the impact strength. The correlation coefficient (R) is 0.98, as determined by carrying out the linear regression analysis.

In another context, effort has been taken to understand the effect of reactive compatibilisation on the morphology and the impact strength of binary and ternary compositions of PA6, EVA and EVA-*g*-MA and to compare the corresponding effect. In all the compositions the dispersed phase concentration was kept at 20 wt% with varying level of EVA-*g*-MA and MA concentration was fixed at 2 wt%. Fig. 16 shows that the increase in impact strength in 80/20, PA6/EVA-*g*-MA (2 wt% MA) is found to be higher than the corresponding ternary compositions in which the maximum

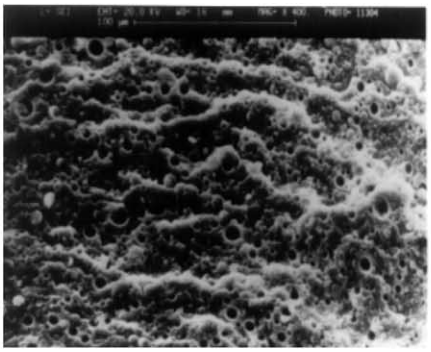

(a) N20

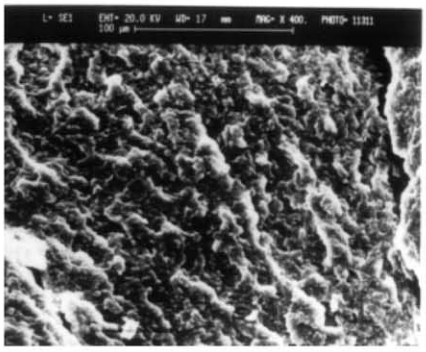

(b) NG1

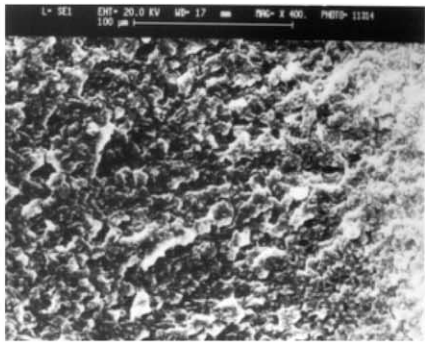

(c) NG2

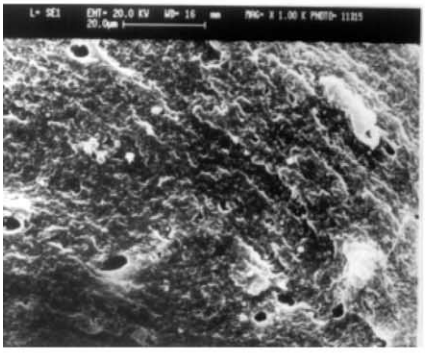

(d) NG4

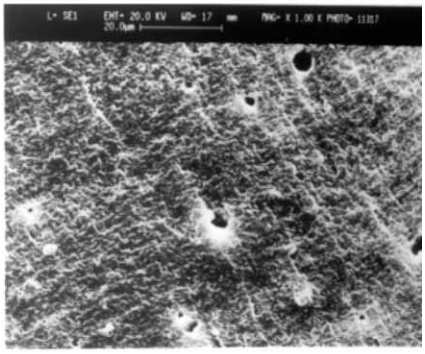

(e) NG6

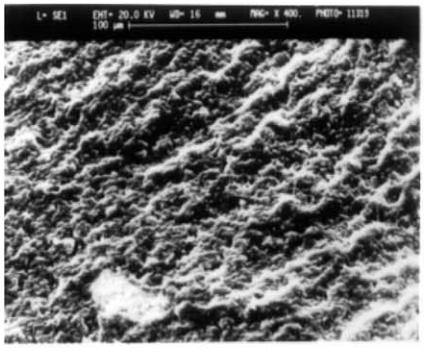

(f) N80E10G10

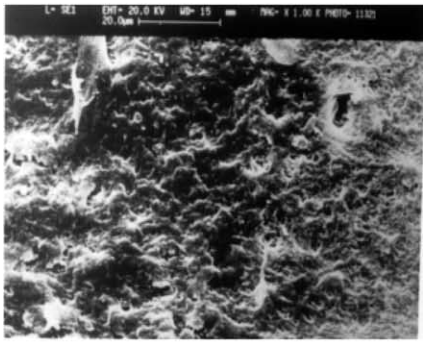

(g) N80E5G15

Fig. 8. Scanning electron micrographs of impact-fractured surfaces of PA6/EVA, PA6/EVA-*g*-MA and PA6/EVA/EVA-*g*-MA blends: (a) N20, (b) NG1, (c) NG2, (d) NG4, (e) NG6, (f) N80E10G10, (g) N80E5G15.

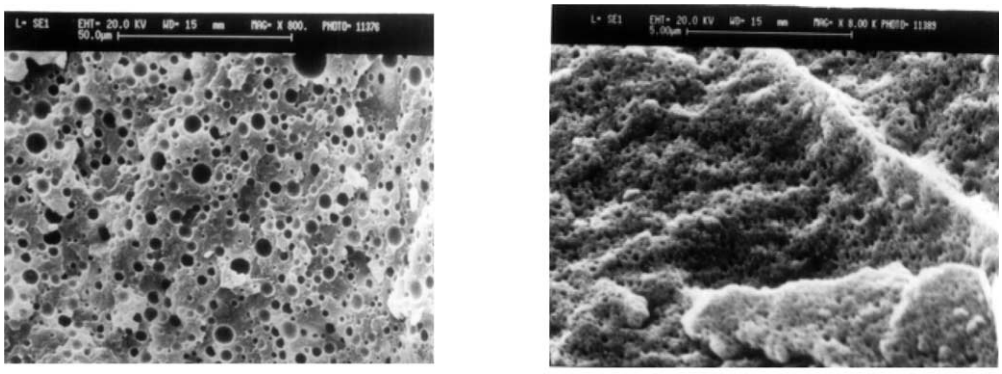

(a) N20 (b) NG4

Fig. 9. Scanning electron micrographs of cryogenically fractured etched surfaces of PA6/EVA and PA6/EVA-*g*-MA blends: (a) N20, (b) NG4.

amount of EVA-*g*-MA concentration was 15 wt%. This can be explained on the basis of average domain size (Fig. 16) in the respective blends and the issue of interfacial saturation. At 20 wt% EVA-*g*-MA level (in PA6/EVA-*g*-MA binary blends), the average domain size is still lower than that of the ternary compositions where maximum amount of EVA-*g*-MA content was 15 wt%, this observation indicates the necessity of morphological stabilisation to achieve higher impact strength. In this context, it is to be mentioned that in case of PET/EPR blends, the addition of EPR-*g*-MA leads to a gradual decrease of the dispersed phase particle size with increasing EPR-*g*-MA level [45].

3.7. Tensile properties

Tensile stress–strain curves are shown in Fig. 17. Various tensile properties such as stress at peak, stress at break and elongation at break determined from these curves are presented in Table 3. It is observed that PA6/EVA blend (N20) exhibits prominent yield point, whereas in the case of PA6/EVA-*g*-MA blends broadening of the yield peak with strain hardening takes place, which is accompanied by lower elongation at break. This observation is more prominent at higher MA level in PA6/EVA-*g*-MA blends. In this context, it is pointed out that the occurrence of strain hardening may be a result of higher entanglements at the interface of PA6 and EVA-*g*-MA phase due to the in situ copolymer formation. However, in the ternary compositions the stress–strain curves are not changing significantly with composition. Similar observations of strain hardening and lower extension at break as compared to PA6 were reported in PA6/EPM-*g*-SA blends [46]. This behaviour was explained on the basis of substantial change induced in the matrix on addition of EPM-*g*-MA, thus making the cold-drawing process of PA6 more difficult [46]. It is observed from the Table 2 that stress at peak increases with increase in MA content in the blend. The increase in stress at peak is 4–17% as MA content increases from 1 to 6 wt%. This increase may be due to better interfacial adhesion between the phases, promoting better stress transfer. It is also observed that the tensile modulus is found to decrease gradually with increase in MA content in EVA-*g*-MA (820 MPa at 0% MA level, 816 MPa at 1%, 805 MPa at 2%, 795 MPa at 4% and 775 MPa at 6% MA level). This might be due to the partial degradation of EVA chain during melt free radical grafting of MA.

3.8. Theoretical analysis of tensile strength (stress at peak)

Theoretical models have been used to analyse the tensile strength data of polymer blends in order to assess the level of interfacial interaction. Kunori and Geil [47] have used such models to analyse the blends of polycarbonate and high-density polyethylene as well as the blends of polycarbonate and polystyrene. Other reported studies also used similar models in polymer blends and composites [48–49]. They have been used to analyse uncompatibilsed PA6/EVA blend in our earlier paper [43]. Three models used to analyse the tensile strength results obtained in this study are as follows:

Model 1: Neilsen's first Power law model [50]:

$$\frac{\sigma_b}{\sigma_p} = (1 - \phi_1)S \tag{4}$$

Model 2: Neilsen's two third Power law model [50]:

$$\frac{\sigma_b}{\sigma_p} = (1 - \phi_1^{2/3})S' \tag{5}$$

Model 3: Nicolais and Narkis model [51]:

$$\frac{\sigma_b}{\sigma_p} = (1 - K_b\phi_1^{2/3}) \tag{6}$$

where σ_b and σ_p represent the tensile strength of the blend and the PA6, respectively, ϕ_1 is the volume fraction of EVA (or EVA-*g*-MA) in the blends. S and S' are the Neilsen's parameter in the first and two third power law models, respectively, which accounts for the weakness in the structure brought about by the discontinuity in stress transfer and generation of stress concentration at the interfaces in case of composites and blends. The maximum

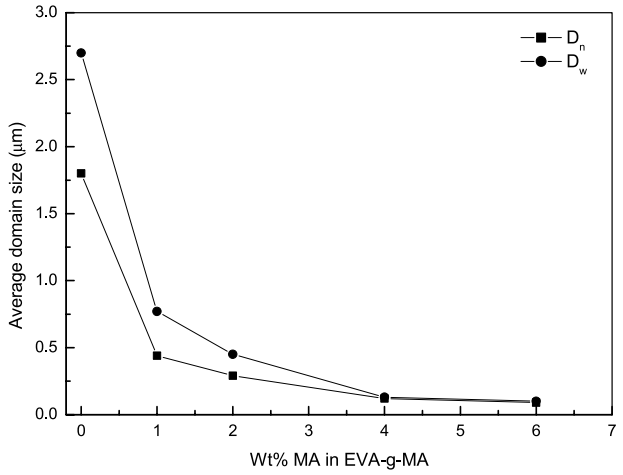

Fig. 10. Variation of average domain size with MA content in EVA-*g*-MA of PA6/EVA-*g*-MA blends.

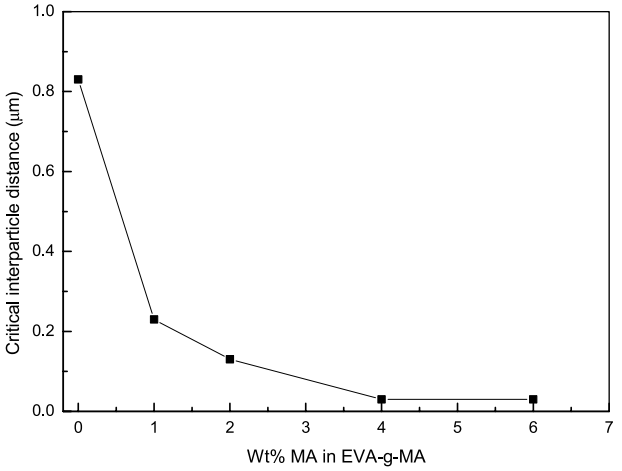

Fig. 12. Variation of critical interparticle distance with MA content in EVA-*g*-MA of PA6/EVA-*g*-MA blends.

value of S and S' is unity for no stress concentration effect. K_b in Eq. (6) is an adhesion parameter; the maximum value of K_b is 1.21 for spherical inclusion of the minor phase having no adhesion [51]. The three models described above have been employed to analyse the tensile strength results in order to evaluate the interfacial adhesion, if any, by comparing the experimental values with those predicted by the models and the results are presented in Table 4. The values of S, S' and K_b are listed in Table 4 giving a comparison between the experimental data and the theoretical models. The minor phase of all these compositions were kept at 20% by weight. It is assumed during the analysis that the density of EVA and EVA-*g*-MA are almost same so that the volume fraction of EVA-*g*-MA remains same as that of pure EVA in the binary compositions. The analysis was made as compared to uncompatibilised 80/20 compositions of PA6/EVA, which has been reported earlier [43]. It was found from the analysis that the experimental values for reactively compatibilised blends are higher than those predicted from the Model 1 taking into account the values of $S=1.00$ and 1.10. The relative tensile strength of all the compositions predicted from Model 1 taking into account $S=1.00$ is found to be 0.76, while the value is found to be 0.84 taking into account of $S=1.10$. The experimental relative tensile strength values of reactively compatibilised blends are found to be higher as compared to the values predicted from Model 1. This shows that all the reactively compatibilised compositions can take excessive stress since the interfacial adhesion has improved as compared to the corresponding uncompatibilised blend. Similarly, the experimental relative tensile strength values are found to be higher as compared to the values predicted from Model 2 taking into account the values of $S'=1.00$ and 1.36. This is again in favour of higher interfacial adhesion in reactively compatibilised blends. Thus, by comparing the values of Neilsen's parameters (S and S') of the two power laws, it is

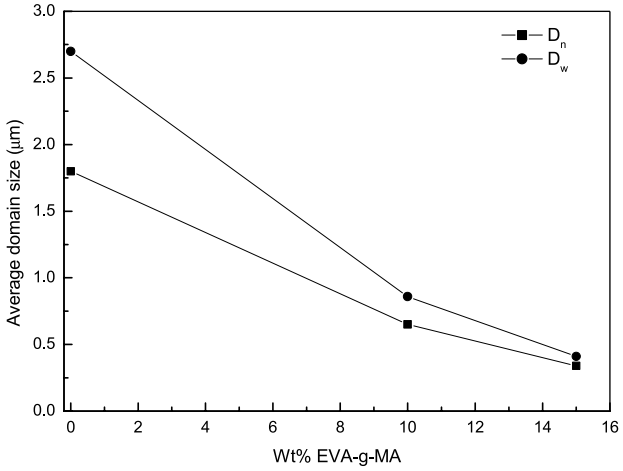

Fig. 11. Variation of average domain size with EVA-*g*-MA content of PA6/EVA/EVA-*g*-MA blends.

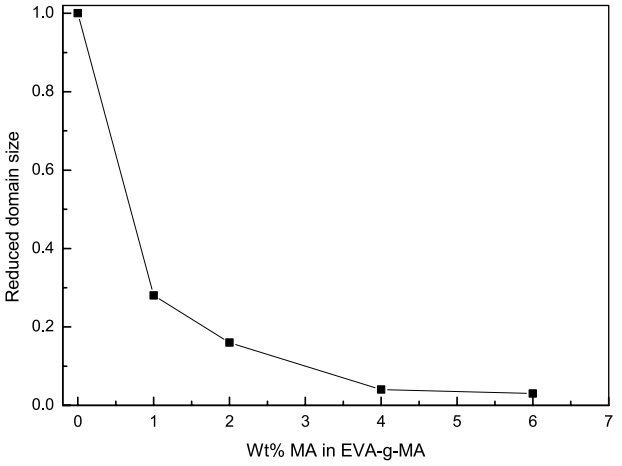

Fig. 13. Plot of reduced domain size versus MA content of PA6/EVA-*g*-MA blends.

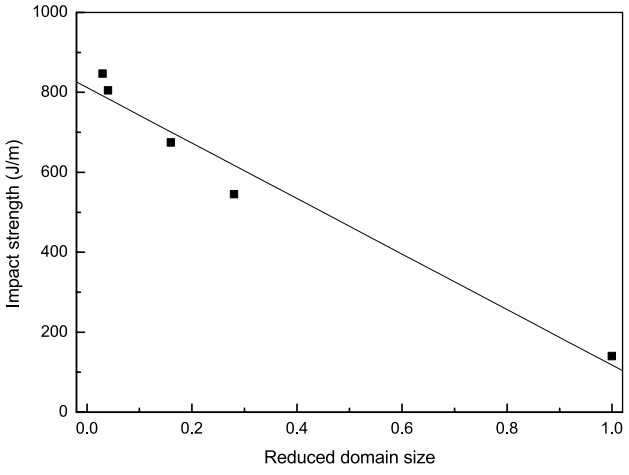

Fig. 14. Plot of impact strength versus reduced domain size of PA6/EVA-*g*-MA blends.

found that the extent of deviation of S value from 1.00 being less than that of S' value, the first power law establishes its better suitability than the fractional power law model. The analysis also shows that the value of K_b for all compositions is much less than 1.21. The dependence of K_b with MA content and with number average domain size of PA6/EVA and PA6/EVA-*g*-MA blends has been plotted in Figs. 18 and 19. It shows that the value of K_b decreases with increasing MA content and with decreasing the average domain size, which once again manifests the effect of reactive compatibilisation on the interfacial adhesion of the PA6/EVA-*g*-MA blends. In an earlier paper on the theoretical analysis of tensile strength of PA6/EVA blends, it was shown that the lowering of interfacial adhesion between PA6 and EVA beyond 20 wt% EVA level was probably due to the coalescence and sequential larger domain size formation of the EVA phase [43]. In this context, it is to be pointed out that the higher interfacial adhesion in PA6/EVA-*g*-MA blends is due to the lowering of rate of coalescence, which has been discussed in the morphology section.

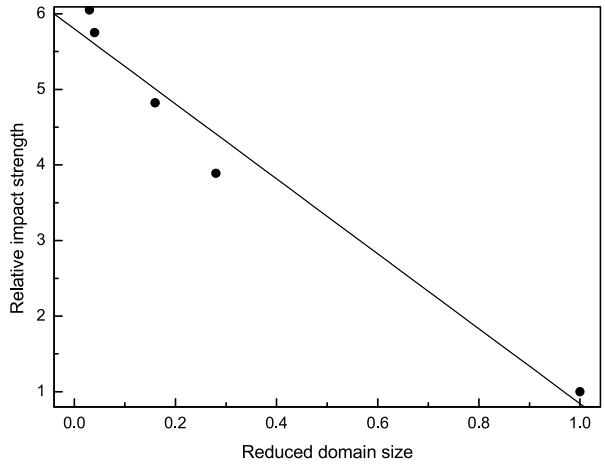

Fig. 15. Plot of relative impact strength versus reduced domain size of PA6/EVA-*g*-MA blends.

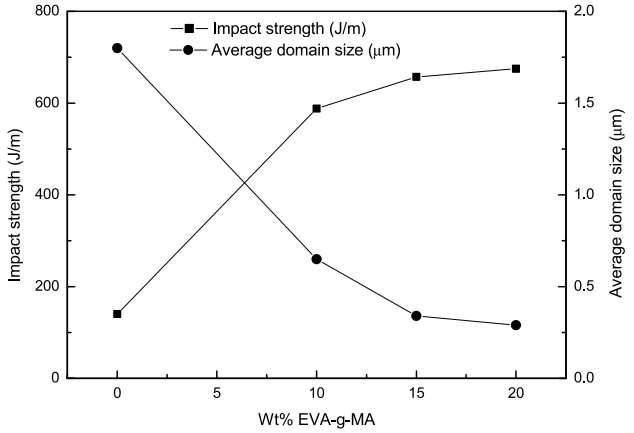

Fig. 16. Variation of impact strength and number average domain size with EVA-*g*-MA content in binary and ternary compositions of PA6, EVA and EVA-*g*-MA.

4. Conclusions

It has been shown earlier that EVA-*g*-MA is an effective compatibiliser for PA6/EVA blends [37]. In the present study the effect of reactive compatibilisation has been demonstrated in the formation of in situ graft copolymer, which leads to the modification of phase morphology thus giving rise to superior mechanical properties of PA6/EVA-*g*-MA and PA6/EVA/EVA-*g*-MA blends. The major conclusions of the present study are as follows:

(i) The formation of EVA-*g*-MA has been identified by FTIR spectroscopy. With increase in initial MA content, the amount of MA grafted onto EVA is found to be higher. In addition, the formation of in situ graft copolymer is identified with the help of ATR-IR

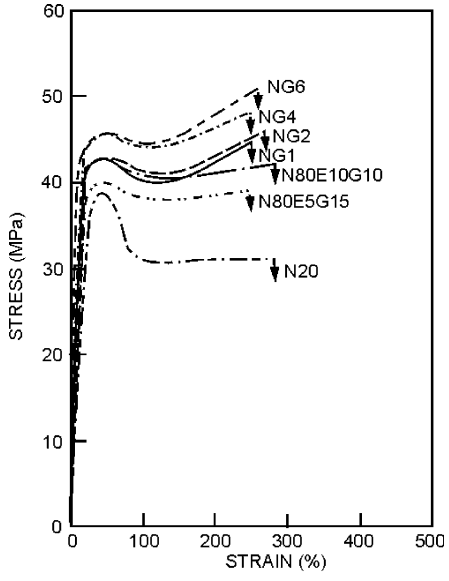

Fig. 17. Stress strain curves of PA6/EVA, PA6/EVA-*g*-MA and PA6/EVA/EVA-*g*-MA blends.

Table 4
Values of stress concentration parameters (S, S' and K_b) in PA6/EVA-*g*-MA blends

Sample[a]	S	S'	K_b
N20	1.01	1.25	0.60
NG1	1.05	1.29	0.53
NG2	1.11	1.38	0.39
NG4	1.17	1.45	0.26
NG6	1.18	1.46	0.26
Mean	1.10	1.36	0.40

[a] Volume fraction of either EVA or EVA-*g*-MA in each sample = 0.233

spectroscopy in extracted samples of PA6 and EVA-*g*-MA blends.

(ii) The overall crystallinity of the reactively compatibilised blends decreased as compared to both uncompatibilised blends and that of pure PA6 which suggests the reduced mobility of crystallising chains due to the graft co-polymer formation at the interface.

(iii) The impact strength increases gradually with increase in MA content and with the level of EVA-*g*-MA in PA6/EVA-*g*-MA and PA6/EVA/EVA-*g*-MA blends, respectively. The brittle to tough transition temperature shifted to 23 °C for these blends as compared to 40 °C for PA6/EVA blends.

(iv) The impact-fractured topology indicates a process of high rate of plastic deformation suggesting better interfacial adhesion.

(v) In the presence of EVA-*g*-MA, the rate of coalescence of the dispersed phase is slower as evidenced by finer and stable dispersion of EVA-*g*-MA domains in PA6 matrix. It is also found that a linear correlation exists between relative impact strength versus reduced domain size, which suggests that reactive compatibilisation is very much effective to improve the impact strength. It is also found that the sufficient amount of compatibiliser is required to stabilise the morphology to achieve higher impact strength.

(vi) The tensile strength of PA6/EVA-*g*-MA and PA6/EVA/EVA-*g*-MA increases significantly as compared to PA6/EVA blends. The theoretical analysis of tensile strength suggests that there is an increase in extent of interaction between PA6 and EVA-*g*-MA, which is also an indication of better interfacial adhesion between PA6 and EVA.

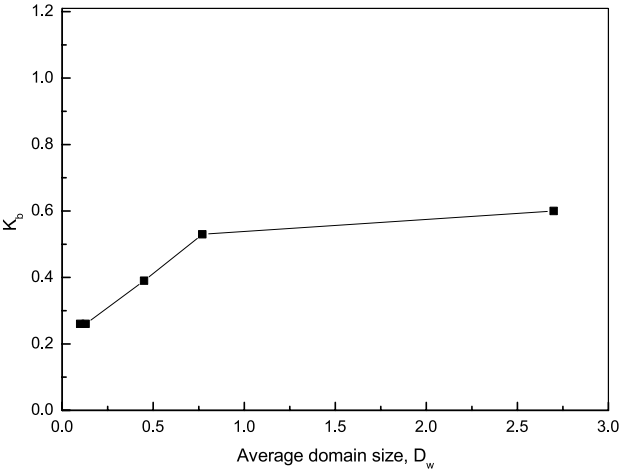

Fig. 19. Variation of K_b with weight average domain size in PA6/EVA-*g*-MA blends.

Acknowledgements

The authors wish to acknowledge the help and support provided to one of the authors (ARB) by Prof. Gabriel Groeninckx for carrying out part of the work in the laboratory of Macromolecular Structural Chemistry, Department of Chemistry, Katholieke University, Leuven, Belgium.

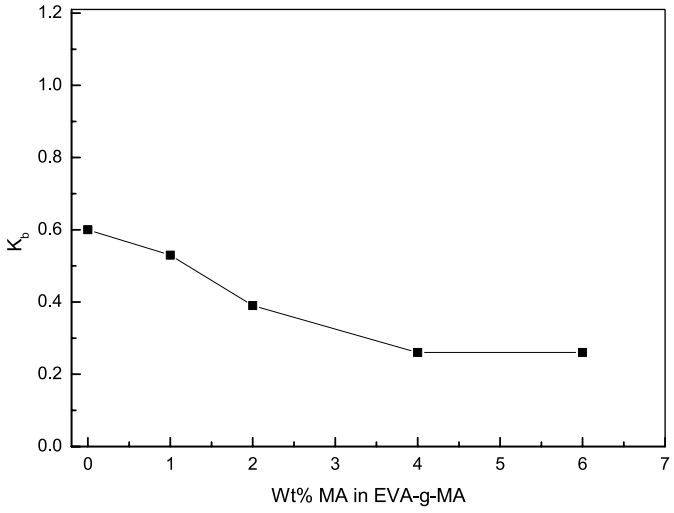

Fig. 18. Plot of K_b versus MA content in EVA-*g*-MA of PA6/EVA-*g*-MA blends.

References

[1] Paul DR, Newman S. Polymer blends. vol. 1. New York: Academic Press; 1979.
[2] Utracki LA, Favis BD. Polymer alloys and blends. In: Cheremisinoff NP, editor. Encyclopedia of engineering materials. NJ: Marcel Dekker; 1988.
[3] Macosko CW, Guegan P, Khandpur AK, Nakayama A, Marechal P, Inoue T. Macromolecules 1996;29:5590.
[4] Sundararaj U, Macosko CW. Macromolecules 1995;28:2647.
[5] Teyssie P, Fyat R, Jerome R. Macromol Chem 1986;187:837.
[6] Thomas S, Groeninckx G. Polymer 1999;40:5799.
[7] Scott CE, Macosko CW. Polymer 1994;35:5422.
[8] Li H, Chiba T, Higashida N, Yang Y, Inoue T. Polymer 1997;38:3921.
[9] Dedecker K, Groeninckx G. Polymer 1998;39:4985.
[10] Dedecker K, Groeninckx G. Polymer 1998;39:4993.
[11] Dedecker K, Groeninckx G. Polymer 1998;39:5001.
[12] Dedecker K, Groeninckx G. Macromolecules 1999;32:2472.
[13] Dedecker K, Groeninckx G. J Appl Polym Sci 1999;73:889.
[15] Charoensirisomboon P, Chiba T, Torikai K, Saito H, Ougizawa T, Inoue T, Weber M. Polymer 1999;40:6975.
[16] Charoensirisomboon P, Chiba T, Inoue T, Weber M. Polymer 2000; 41:5977.
[17] Okamoto M, Inoue T. Polym Eng Sci 1993;33:175.
[18] Wu S. Polymer 1985;26:1855.
[19] Wu S. Polym Eng Sci 1987;27:335.
[20] Borggreve RJM, Gaymans RJ. Polymer 1989;30:63.
[21] Borggreve RJM, Gaymans RJ, Schuijer J. Polymer 1989;30:71.
[22] Borggreve RJM, Gaymans RJ, Schuijer J, Ingen Housz JF. Polymer 1987;28:1489.
[23] Oshinski AJ, Keskkula H, Paul DR. Polymer 1996;37:4891.
[24] Oshinski AJ, Keskkula H, Paul DR. Polymer 1996;37:4909.
[25] Oshinski AJ, Keskkula H, Paul DR. Polymer 1996;37:4919.
[26] Seo Y, Ninh TH. Polymer 2004;45:8573.
[27] Wu D, Wang X, Jin R. Eur Polym J 2004;40:1223.
[28] Tol RT, Groeninckx G, Vinckier I, Moldenaers P, Mewis J. Polymer 2004;45:2587.
[29] Martin P, Gallez C, Devaux J, Legras R, Leemans L, van Gurp M, van Duin M. Polymer 2003;44:5251.
[30] Scaffaro R, La Mantia FP, Canfora L, Polacco G, Filippi S, Magagnini P. Polymer 2003;44:6951.
[31] Nitayama N, Keskkula H, Paul DR. Polymer 2001;42:3751.
[32] Wang X, Li H, Ruckenstein E. Polymer 2001;42:9211.
[33] Puyvelde PV, Oommen Z, Koets P, Groeninckx G, Moldenaers P. Polym Eng Sci 2003;43:71.
[34] Kim SJ, Kim DK, Cho WJ, Ha CS. Polym Eng Sci 2003;43:1298.
[35] Legros A, Carreau PJ, Favis BD, Michel A. Polymer 1994;35:758.
[36] Legros A, Carreau PJ, Favis BD, Michel A. Polymer 1997;38:5085.
[37] Bhattacharyya AR, Ghosh AK, Misra A. Polymer 2001;42:9143.
[38] Kim SJ, Kang CJ, Chowdhury SR, Cho WJ, Ha CS. J Appl Polym Sci 2003;89:1305.
[39] Kim SJ, Shin BS, Hong JL, Cho WJ, Ha CS. Polymer 2001;42:4073.
[40] Cartier H, Hu GH. J Polym Sci Part A: Polym Chem 1998;36:1053.
[41] Cartier H, Hu GH. J Polym Sci, Part A: Polym Chem 1998;36:2763.
[42] Hu GH, Sun YJ, Lambla M. Polym Eng Sci 1996;36:676.
[43] Bhattacharyya AR, Maiti SN, Misra A. J Appl Polym Sci 2002;85: 1593.
[44] Speroni F, Castoldi E, Fabbri P, Casiraghi T. J Mater Sci 1989;24: 2165.
[45] Loyens W, Groeninckx G. Macromol Chem Phys 2002;203:1702.
[46] Cimmino S, D'Orazio L, Greco R, Maglio G, Malinconico M, Mancarella C, et al. Polymer 1984;24:48.
[47] Kunori T, Geil PH. J Macromol Sci Phys 1980;B18:135.
[48] Gupta AK, Purwar SN. J Appl Polym Sci 1984;29:3513.
[49] Maiti SN, Lopez BH. J Appl Polym Sci 1992;44:353.
[50] Neilsen LE. J Appl Polym Sci 1966;10:97.
[51] Nicolais L, Narkis M. Polym Eng Sci 1971;1:194.